


Two-dimensional oxides assembled by  $M_4$  clusters ( $M = \text{B, Al, Ga, In, Cr, Mo, and Te}$ )

Yu Guo, Qiuying Du, Pengju Wang, Si Zhou,\* and Jijun Zhao†

Key Laboratory of Materials Modification by Laser, Ion and Electron Beams (Dalian University of Technology),  
Ministry of Education, Dalian 116024, China (Received 22 June 2021; revised 27 October 2021; accepted 6 December 2021; published 30 December 2021)

Cluster-assembled materials have long been pursued as they provide unprecedented opportunities to integrate desired functionalities in technological devices. However, patterning clusters in ordered phases in avoid of agglomeration remains challenging. Here we propose a strategy to construct stable two-dimensional (2D) superlattices by using tetrahedral clusters covalently linked by oxygen atoms. When satisfying the closed shells of both molecular and atomic orbitals for the clusters and oxygen linkers, respectively, the assembled 2D superlattices exhibit outstanding energetic, dynamic, and thermal stabilities. Following these criteria, monolayers of  $\text{B}_4\text{O}_2$ ,  $\text{Al}_4\text{O}_2$ ,  $\text{Ga}_4\text{O}_2$ ,  $\text{In}_4\text{O}_2$ ,  $\text{Cr}_4\text{O}_2$ ,  $\text{Mo}_4\text{O}_2$ , and  $\text{Te}_4\text{O}_2$  were assembled, which possess application-desired physical properties, such as moderate band gaps, small carrier effective masses, and strong optical absorption in the visible regime. These critical insights pave a new avenue to fabricate new materials and devices using cluster building blocks with precise structures and functionalities.

DOI: [10.1103/PhysRevResearch.3.043231](https://doi.org/10.1103/PhysRevResearch.3.043231)

## I. INTRODUCTION

Nowadays, two-dimensional (2D) atomic crystals, such as graphene, silicene, group-V monolayers, etc., are raising increasing attention for their extraordinary physical properties in terms of electronic band structure, charge-carrier mobility, and magnetic and optical properties [1–7]. Extensive experimental and theoretical efforts have been made to design and synthesize novel 2D crystals with unprecedented functionalities for technological devices [8–12]. Compared with individual atoms, subnanometer clusters can serve as building blocks with highly modulatable electronic structures for assembling 2D materials and devices [13,14]. As the structures and fundamental properties of clusters vary with their sizes, compositions, oxidation states, and the emergent behavior sensitively depend on their architecture, the cluster assemblies offer the attractive proposition of sculpturing nanostructures with the combinations of desired functionalities [15–17].

To date, some cluster-assembled nanomaterials have been synthesized in the experiment. For instance, CdTe magic-sized clusters were assembled into 2D quantum confined nanoplatelets with the growth process influenced by the presence of long hydrocarbon chain primary amines [18]. The van der Waals (vdW)  $\text{Re}_6\text{Se}_8$  clusters were assembled into a 2D hierarchical semiconductor, exhibiting tunable transport properties from semiconductor to metallic behavior and to superconductor upon  $n$  doping through Cl dissociation [19–21].  $\text{Ag}_{12}$  clusters were successfully assembled into a periodic

crystal in the trigonal space group by linking with bidentate pyridine ligands with luminescence regulated by adjusting the structure of clusters and ligand species [22].  $\text{C}_{60}$  with  $\text{Co}_6\text{Se}_8/\text{Cr}_6\text{Te}_8/\text{Ni}_6\text{Te}_8$  clusters were patterned into a simple crystalline array, such as the  $\text{CdI}_2$  structure type [23,24]. On the theoretical side, Du *et al.* examined 27 dimers of endohedral cage clusters and predicted that  $M@X_{16}$  ( $M = \text{Ti, Zr, or Hf}$ ;  $X = \text{Si, Ge, or Sn}$ ) are potential zero-dimensional vdW Lego blocks [25]. The assembled 2D superlattices exhibit rich electronic band structures from doped semiconductors to antiferromagnetic Mott insulators. They also proposed several stringent criteria for searching clusters as vdW-type building blocks in terms of geometrical and electronic structures.

Among the clusters, “superatoms” possess extraordinary stability and are most promising for assembling nanostructures and solids. As described by the jellium model, molecular orbitals generated by the valence electrons in highly symmetric clusters have shapes just like atomic orbitals. Therefore, a cluster will have enhanced stability when its number of valence electrons coincides with a closed-shell structure (namely, magic number), and the cluster is called a superatom. For clusters with lower symmetries, the molecular orbitals split in energy. The splitting pattern is related to the structural symmetry and can be completely determined by the point-group theory. Some more sophisticated theories based on the shell model have been developed, such as the symmetry-adapted orbital model [26], which explicitly illustrates the electronic configurations of clusters with  $I_h$ ,  $O_h$ , and  $T_d$  symmetries and the corresponding magic numbers.

As one of the simplest superatoms, the tetrahedral  $\text{P}_4$  cluster with  $T_d$  symmetry has the magic number of 20 valence electrons in its ground state [26].  $\text{P}_4$  is the building block of the most stable solid allotropes of phosphorus. The best-known white phosphorus is composed of  $\text{P}_4$  molecules, which transforms to the red phosphorus under heat, light, or X-radiation.  $\text{P}_4$  is also an important unit of liquid phosphorus formed at moderate temperatures [27]. The black phosphorus

\*Corresponding author: [sizhou@dlut.edu.cn](mailto:sizhou@dlut.edu.cn)†Corresponding author: [zhaojj@dlut.edu.cn](mailto:zhaojj@dlut.edu.cn)

layer can be regarded as deformed  $P_4$  clusters covalently linking with each other [28].

Inspired by the  $P_4$  molecule, herein we proposed a simple rule for constructing stable 2D materials by using tetrahedral clusters ( $M_4$ ) covalently linked by O atoms. This cluster-assembling rule takes into account both the closed electronic shells for the  $M_4$  cluster and O atom as well as the electron transfer between them. According to this, the tetrahedral clusters of group-IIIA (B, Al, Ga, and In), group-VIB (Cr and Mo) and group-VIA (Te) elements are suitable building blocks to form stable oxide monolayers with a chemical formula of  $M_4O_2$ , which are indeed verified by our high-throughput screening of the periodic table and global optimization of crystal structures by the CALYPSO methodology. The dynamical and thermal stabilities of these cluster-assembled 2D monolayers were assessed, and their electronic properties were discussed. The molecular orbitals and superatom characters of the tetrahedral clusters were examined to gain deep insights into their high stability and bonding nature with O atoms. These findings open a route for the discovery of 2D atomic crystals and provide useful building blocks for the bottom-up design of functional materials.

## II. COMPUTATIONAL METHODS

Density functional theory calculations [29] were performed by using the Vienna *ab initio* simulation package (VASP) [30]. We used the plane-wave basis set with an energy cutoff of 500 eV [31], the projector augmented-wave potentials [32], and the generalized gradient approximation (GGA) parameterized by Perdew, Burke, and Ernzerhof (PBE) for the exchange–correlation functional [33]. Since the conventional GGA functionals, such as PBE usually underestimate the band gap, a hybrid HSE06 functional [34] was used to compute the electronic structures and optical absorption properties of the assembled sheets. The convergence criteria for total energy and force were set to  $10^{-7}$  eV and  $0.01 \text{ eV}\text{\AA}^{-1}$ , respectively. Uniform  $\mathbf{k}$ -point meshes with spacing of  $\sim 0.015 \text{\AA}^{-1}$  were adopted to sample the 2D Brillouin zones. A vacuum region of  $15 \text{\AA}$  was added to the vertical direction to avoid interactions between the neighboring layers. Phonon dispersion analysis was performed by using the PHONOPY code interfaced with the density functional perturbation theory [35] as implemented in VASP. The electron density of the frontier molecular orbitals and natural population of the on-site charge were calculated using the PBE functional accompanied with  $6-311 + G(d)$  [36] and SDD [37] basis sets, implemented in the GAUSSIAN16 package [38]. The particle-swarm optimization (PSO) method implemented in the CALYPSO code [39,40] was employed to search for low-energy structures of  $(M_2O)_n$  ( $n = 1 - 3$ ) monolayers. In our PSO search, both the population size and the number of generations were set to 30. The required structural relaxations were performed by using the PBE functional.

## III. RESULTS AND DISCUSSION

To explore the possible cluster-assembling rules, we consider a simple square lattice formed by the tetrahedral  $M_4$  clusters each coordinated with four O atoms as shown in

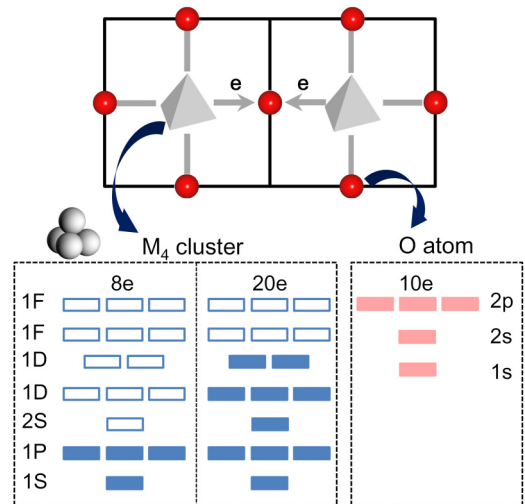


FIG. 1. Schematic for assembling  $M_4O_2$  monolayer structures by using tetrahedral  $M_4$  clusters and O atoms. Thick gray arrows represent electron transfer. The required electronic structures of  $M_4$  clusters and O atoms for assembling stable 2D superstructures are shown in the bottom panels.

Fig. 1. There will be electron transfer from  $M_4$  clusters to the neighboring O atoms. To reach a stable electronic structure for the whole monolayer, each  $M_4$  cluster should retain a magic number of electrons (8, 20, 34, 40, etc.) to satisfy a closed electronic shell following the symmetry-adapted orbital model [26,41] as illustrated in Fig. 1. The O linkers should have their atomic orbitals fully filled, which requires the gaining of two electrons from  $M_4$  clusters. This further indicates that the difference of electronegativity between  $M$  and O atoms should be sufficient large to guarantee the electron transfer to form strong  $M - O$  bonds.

According to the above criteria, group-IIIA atoms (B, Al, Ga, In, and Tl) have the electronic configuration for valence electrons of  $s^2p^1$ . Their tetrahedral clusters will carry eight valence electrons after donating four electrons to the two neighboring O atoms in the unit cell, satisfying the magic number of tetrahedral clusters with fully occupied superatom orbitals of  $1S^21P^6$ . As Tl is highly toxic and pollutant, the assembled  $Tl_4O_2$  monolayer will not be discussed in the following content (its stable phonon dispersions and good thermal stability are demonstrated in Fig. S1 of the Supplemental Material [42]). The group-VIB atoms (Cr, Mo, and W) and group-VIA atom (Te) can also meet the above requirement, which have six valence electrons with the electronic configurations of  $d^5s^1$  ( $d^4s^2$  for W) and  $s^2p^4$ , respectively. The  $M_4$  clusters of these elements will carry 20 electrons upon the donation of four electrons to the two O linkers in the unit cell, endowing the  $M_4$  cluster with a closed electronic shell of  $1S^21P^62S^21D^{10}$ . The nonmetallic elements S and Se are excluded as their electronegativity is close to that of O and would not be suitable to form oxide monolayers.

The structural optimization confirms the stable 2D assembled monolayers of  $B_4O_2$ ,  $Al_4O_2$ ,  $Ga_4O_2$ ,  $In_4O_2$ ,  $Cr_4O_2$ ,  $Mo_4O_2$ , and  $Te_4O_2$ , as displayed in Fig. 2. Their geometrical parameters are given by Table I. The  $B_4O_2$ ,  $Al_4O_2$ ,  $Ga_4O_2$ , and  $In_4O_2$  monolayers possess a square lattice with  $p4m$  plane

TABLE I. Lattice parameters  $a$  and  $b$  (Å), bond length  $l$  (Å), and bond angle  $\theta$  ( $^\circ$ ) of  $M_4$  clusters in the 2D assembled crystals, bond overlap population  $\beta$  of the  $M - O$  bond, the number of valence electrons for  $M$  ( $CT_M$ ) and O ( $CT_O$ ) atoms, formation energy  $\Delta H$  (eV/atom), band-gaps  $E_g$  (eV), and carrier effective masses for holes  $m_h$  and electrons  $m_e$  (in the unit of  $m_0$ ,  $m_0$  is the electron rest mass) for assembled  $M_4O_2$  monolayers. The symbol “ $d$ ” in parentheses indicates a direct band gap, and “ $x$ ” and “ $y$ ” indicate effective masses along the  $x$  and  $y$  directions, respectively.

	B <sub>4</sub> O <sub>2</sub>	Al <sub>4</sub> O <sub>2</sub>	Ga <sub>4</sub> O <sub>2</sub>	In <sub>4</sub> O <sub>2</sub>	Cr <sub>4</sub> O <sub>2</sub>	Mo <sub>4</sub> O <sub>2</sub>	Te <sub>4</sub> O <sub>2</sub>
$a$	4.11	5.79	6.08	7.11	2.80	3.08	6.14
$b$					9.70	10.67	11.64
$l$	~1.70	~2.62	~2.70	~3.20	2.20–2.70	2.50–2.99	2.74–3.28
$\theta$	~60	~60	~60	~60	58–71	51–69	49–66
$\beta$	0.67	0.46	0.46	0.45	0.67	0.61	0.55
$CT_M$	2.14	2.21	2.25	2.29	5.27	5.34	5.25
$CT_O$	7.85	7.80	7.76	7.71	7.75	7.79	7.87
$\Delta H$	−0.79	−0.90	−0.55	−0.31	−0.45	−0.38	−0.45
$E_g$	4.26	3.11 ( $d$ )	3.39 ( $d$ )	2.84 ( $d$ )			1.49
$m_h$	1.54	0.52	6.36	1.01			0.78 ( $x$ ) 0.26 ( $y$ )
$m_e$	5.33	3.07	3.51	3.68			0.24 ( $x$ ) 0.33 ( $y$ )

symmetry group [43]. The lattice parameter  $a$  in the range of 4.11–7.11 Å increases with the atomic number of  $M$ . Monolayer Te<sub>4</sub>O<sub>2</sub> exhibits a lower symmetry of the  $cm$  plane group [43] with orthorhombic lattice parameters of 6.14 and 11.64 Å along the  $x$  and  $y$  directions, respectively. Cr<sub>4</sub>O<sub>2</sub> and Mo<sub>4</sub>O<sub>2</sub> monolayers with the  $cm$  2D plane symmetry group [43] also have an orthorhombic structure with lattice parameters of 2.80 and 3.08 Å along the  $x$  direction and 9.70 and 10.67 Å along the  $y$  direction, respectively. In particular, the  $d$  orbitals of adjacent Cr<sub>4</sub> or Mo<sub>4</sub> clusters in the oxide layers are prone to overlap to form  $\delta$  bonds [44–46], yielding an edge-sharing geometry along the  $x$  direction as depicted in Fig. 2(b). Also with six valence electrons, the tetrahedral cluster of W can be assembled into the same 2D oxide structure as that of Cr<sub>4</sub>O<sub>2</sub> and Mo<sub>4</sub>O<sub>2</sub>. However, the phonon dispersion of the W<sub>4</sub>O<sub>2</sub> monolayer is not stable, showing imaginary phonon band and meaning that it is dynamically unstable (see Fig. S2 of the Supplemental Material) [42]. This may be related to the  $6s^2$  outermost shell of W, making it unfavorable to share electrons with O atoms compared with Cr and Mo. For all the other metallic elements in the periodic table, the 2D superlattices of  $M_4$  clusters linked by O atoms are not stable upon structure

optimization. They either collapse during the structural relaxation, or form compounds with O atoms without retaining the  $M_4$  cluster feature (as displayed in Fig. S3 of the Supplementary Material [42]), implying the necessity of satisfying the magic numbers of  $M_4$  clusters with O linkers for assembling stable 2D structures.

The bond nature and charge transfer between  $M_4$  cluster and O linker are analyzed. The bond overlap population [47] of  $M - O$  bonds in the assembled  $M_4O_2$  monolayers ranges from 0.45 to 0.67, suggesting the covalent nature of  $M - O$  bonds. The Bader charge analysis further confirms that the O, group-III A, group-VI B, and Te atoms in the  $M_4O_2$  monolayers each carries about eight, two, five, and five valence electrons (Table I), respectively. This manifests our proposed assembling rule of electronic-shell closure for the O atoms and tetrahedral  $M_4$  clusters, i.e., eight electrons for B<sub>4</sub>, Al<sub>4</sub>, Ga<sub>4</sub>, and In<sub>4</sub>, and 20 electrons for Cr<sub>4</sub>, Mo<sub>4</sub>, and Te<sub>4</sub> after charge transfer with O linkers. Note that free Al<sub>4</sub>, Mo<sub>4</sub>, and Cr<sub>4</sub> clusters have the tetrahedral structures as the ground state [48–50], whereas free B<sub>4</sub>, Ga<sub>4</sub>/In<sub>4</sub>, and Te<sub>4</sub> clusters favor the planar rhombic, rhombic squared, and orthorhombic geometries, respectively [51–53]. We have used the  $M_4$  clusters of their ground-state structures to construct the 2D assembled models. However, they all relax to the tetrahedral configurations shown in Fig. 2 upon structural optimization, indicating the preference for the  $T_d$  symmetry when  $M_4$  clusters carry the magic number of electrons in the assembled oxide monolayers.

To characterize the thermodynamic stability of the assembled  $M_4O_2$  monolayers, we define the formation energy  $\Delta H$  as

$$\Delta H = (E_{\text{tot}} - n_1 \times E_M - n_2 \times E_O)/n, \quad (1)$$

where  $E_{\text{tot}}$  is the energy of  $M_4O_2$  monolayer;  $E_M$  and  $E_O$  are the energies of a  $M$  atom in its solid phase and an O atom in the gaseous O<sub>2</sub> molecule, respectively;  $n_1$  and  $n_2$  are the numbers of atoms of each element in the unit cell of  $M_4O_2$  monolayers, and  $n$  is the total number of atoms in the unit cell. All the  $M_4O_2$  monolayers show negative  $\Delta H$

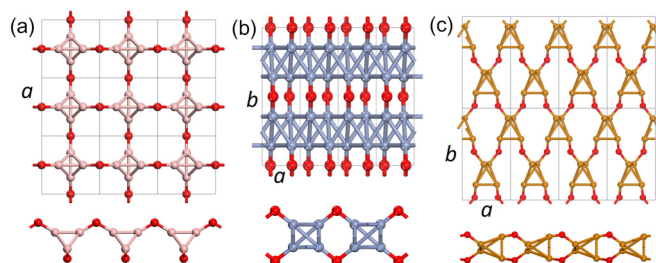


FIG. 2. Atomic structures of cluster-assembled oxide monolayers: (a) B<sub>4</sub>O<sub>2</sub>, Al<sub>4</sub>O<sub>2</sub>, Ga<sub>4</sub>O<sub>2</sub>, and In<sub>4</sub>O<sub>2</sub>; (b) Cr<sub>4</sub>O<sub>2</sub> and Mo<sub>4</sub>O<sub>2</sub>; (c) Te<sub>4</sub>O<sub>2</sub>. The top and bottom panels are the top and side views, respectively. The lattice constants  $a$  and  $b$  are indicated by black boxes. The B/Al/Ga/In, Cr/Mo, Te, and O atoms are shown in pink, blue, brown, and red colors, respectively.

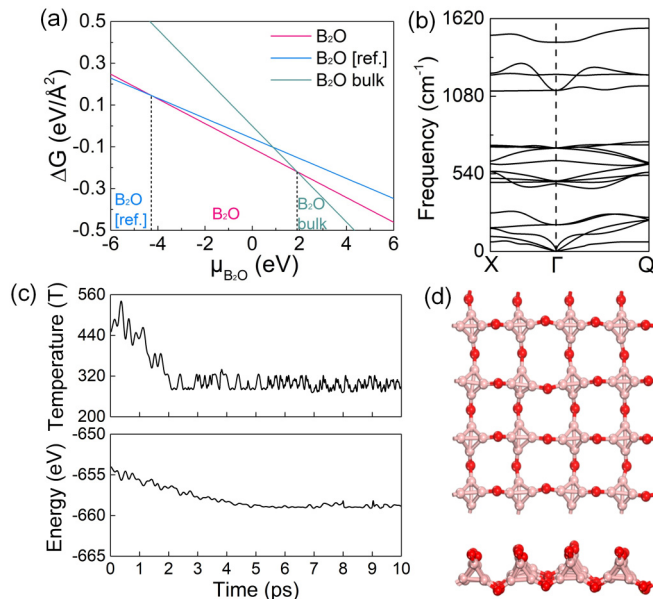


FIG. 3. (a) Chemical potential phase diagram of surface free energy in the unit of area at the  $xy$  plane for our predicted  $B_4O_2$  structure (pink line), previously proposed  $B_2O$  monolayer (blue line), and bulk  $B_2O$  structure (green line). (b) Phonon dispersion of  $B_4O_2$  monolayer as a representative. (c) Variations of temperature and energy with the time of AIMD simulation for the  $B_4O_2$  monolayer. (d) Snapshots of the equilibrium structures of monolayer  $B_4O_2$  (or  $Al_4O_2$ ,  $Ga_4O_2$ , and  $In_4O_2$ ) from AIMD simulations with temperature controlled at 300 K.

of  $-0.25$  to  $-0.90$  eV per atom, suggesting that their formation is exothermic. In particular, there are several reported stable phases of the  $B_2O$  monolayer from both experiment and theory, whose stability can be compared with our predicted assembled materials. Note that the previously proposed  $B_2O$  monolayer [54,55] and  $B_2O$  bulk system [56] in Fig. S4 of the Supplemental Material [42] have formation energies of  $-0.69$  and  $-0.49$  eV/atom, respectively, both higher than that of our proposed  $B_4O_2$  structure ( $-0.79$  eV/atom). Figure 3(a) plots the free-energy ( $\Delta G$ ) curves for various  $B_2O$  source conditions, demonstrating the easy formation of the present  $B_4O_2$  monolayer with the chemical potential of  $\mu_{B_2O}$  in a rather wide range of  $-4.28$  eV to  $1.90$  eV. Therefore, the cluster-assembled  $B_4O_2$  monolayer can exist in the experimental condition with moderate supply of B and O atoms.

The dynamic stability of the assembled seven  $M_4O_2$  monolayers is confirmed by their phonon dispersions without imaginary bands as shown in Figs. 3(b) and S5 of the Supplemental Material [42]. We also performed *ab initio* molecular dynamics (AIMD) simulations [57] to assess their thermal stability [see Figs. 3(c), 3(d), and S6 of the Supplemental Material] [42]. The evolution of the energy and temperature with the simulation time is plotted in Fig. 3(c). After 10 ps of AIMD simulations, all the  $M_4O_2$  monolayers well maintain their planar structures at 300 K. To further confirm the relative stability of the cluster-assembled 2D materials among various structure phases of the same stoichiometry, we employed the CALYPSO code to search the most stable structures of 2D  $B_4O_2$  and  $Te_4O_2$  as representatives. After a systematic structural

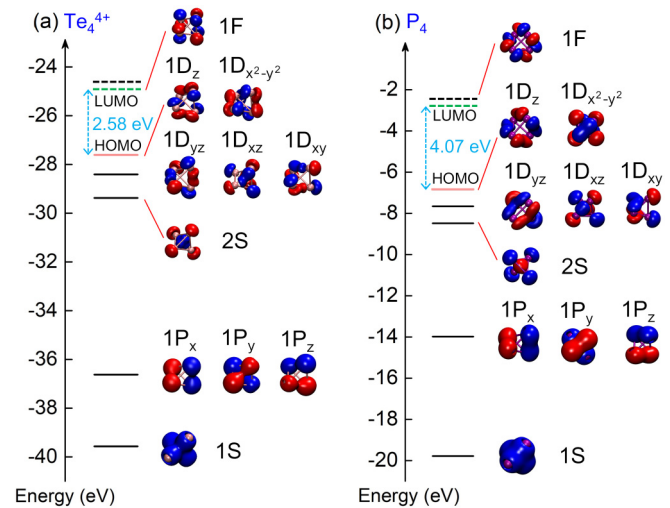


FIG. 4. Molecular orbitals referred to the vacuum energy level as zero and a classification of orbital pattern into superatomic 1S, 1P, 1D, 2S, and 1F states for (a)  $Te_4^{4+}$  and (b)  $P_4$  cluster. The solid and dashed lines refer to occupied and unoccupied orbitals, respectively. Blue and red colors denote positive and negative phases of the wave function, respectively. The isosurface value is  $\pm 0.05$  a.u.

search, hundreds of isomers were generated with four representative low-lying geometries presented in Fig. S7 of the Supplemental Material [42]. Intriguingly, the global minimum search by the CALYPSO code produced the same geometrical structures of  $B_4O_2$  and  $Te_4O_2$  monolayers as we predicted above. All these results support that our proposed assembling rule can indeed serve as a compass to construct new 2D materials in the ground state and having outstanding dynamic and thermal stabilities, which thus are promising to realize in the experiment.

To gain further insights into the high stability of the present cluster-assembled 2D oxide monolayers, we examined the molecular orbitals of a free  $Te_4^{4+}$  cluster in the tetrahedral geometry. Its electronic configuration resembles that in the  $Te_4O_2$  monolayer with each  $Te^+$  species ( $2s^22p^3$ ) holding about five valence electrons upon the donation of one electron to a O atom. As demonstrated in Fig. 4, the  $Te_4^{4+}$  cluster with high symmetry exhibits the superatomic characteristics. Compared with  $P_4$ , the  $Te_4^{4+}$  cluster has a smaller highest occupied molecular orbital-lowest unoccupied molecular orbital (HOMO-LUMO) gap of 2.58 eV and much deeper energy level due to the positive charges carried by the cluster. Remarkably, the  $Te_4^{4+}$  cluster presents the highly symmetric superatomic orbital properties with valence electron configuration of  $1S^21P^62S^11D^{10}||1P^0$  (the double vertical line separates the gap between occupied and unoccupied orbitals). The superatomic behavior of  $Te_4^{4+}$  is similar to its isoelectronic counterpart (i.e.,  $P_4$ ), which satisfies the requirement of closed electronic shells.

It is worth mentioning that the jellium model treats the cluster as a positively charged ionic core surrounded by free-electron-like valence electrons [58,59]. It assumes not only a delocalized nature of valence electrons, but also a small atomic core of the cluster compared to atomic volume with a weak core potential [41]. The jellium model is mostly



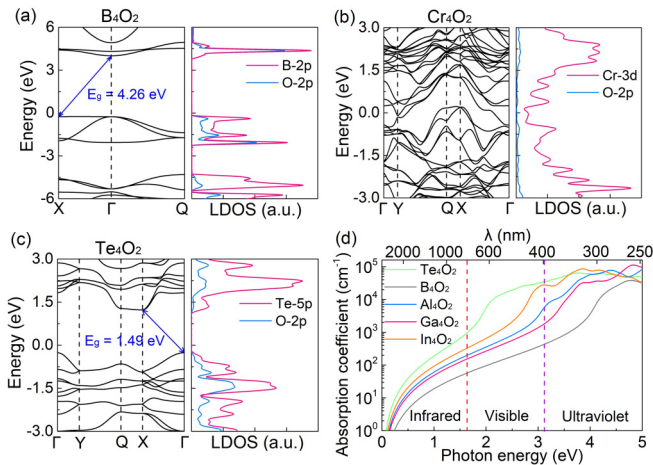


FIG. 5. (a)–(c) Electronic band structures and local density of states (LDOS) for  $B_4O_2$ ,  $Cr_4O_2$ , and  $Te_4O_2$  monolayers, respectively.  $E_g$  is the band gap denoted by solid blue arrow. High-symmetry points in the first Brillouin zone are  $\Gamma$  (0,0,0),  $Y$  (0,0.5,0),  $Q$  (0.5,0.5,0), and  $X$  (0.5,0,0). (d) Optical absorption coefficients for  $B_4O_2$ ,  $Al_4O_2$ ,  $Ga_4O_2$ ,  $In_4O_2$ , and  $Te_4O_2$  monolayers.  $\lambda$  is the wavelength of light. The area between the red and the purple dashed lines represents the visible range.

applicable for simple metal clusters, coinage metal clusters, and ligated clusters. Here, the tetrahedral  $M_4$  clusters of group-III A elements should fulfill the above requirements by the jellium model. The localization degree of valence electrons can be described by the electron localization function (ELF) [60,61]. The ELF takes values in the range of 0 to 1, where 1 corresponds to perfect localization and 0.5 corresponds to perfect delocalization. For the assembled  $B_4O_2$ ,  $Al_4O_2$ ,  $Ga_4O_2$ , and  $In_4O_2$  monolayers, all their ELF reveals a delocalized behavior of electron density encompassing the whole  $M_4$  cluster instead of localizing on individual atoms with ELF values around 0.5 in the regions between  $M$  ions (see Fig. S8 in the Supplemental Material for details) [42]. Therefore, the jellium model is valid for the group-III A  $M_4O_2$  monolayers. On the other hand, the core potential is not weak in  $Cr_4$ ,  $Mo_4$ , and  $Te_4$  clusters. The ELF is about 0.8 in the assembled  $Cr_4O_2$ ,  $Mo_4O_2$ , and  $Te_4O_2$  monolayers, indicating some localization of the valence electrons. Nevertheless, the high symmetry of  $M_4$  clusters leads to an ordering pattern of electronic levels similar to that of the jellium model but with shell splitting and even reverse order between shells. A complete filling of the electronic shells renders the  $M_4$  clusters with superatom characteristics based on the shell model [62] and, thus, results in high stability for the assembled  $M_4O_2$  monolayers. Besides the electronic configuration, a cluster's stability can also be associated with aromaticity, HOMO-LUMO gap, spin excitation energy, the presence of ligands, and so on [61,63–66]. These factors have to be carefully taken into account when assembling clusters of other symmetries into certain superlattices.

The electronic band structures of the assembled  $M_4O_2$  monolayers are presented in Fig. 5 and Fig. S9 of the Supplemental Material [42], and their theoretical band gaps at the HSE06 level are given in Table I.  $Cr_4O_2$  and  $Mo_4O_2$

exhibit typical metallic character. In contrast,  $B_4O_2$ ,  $Al_4O_2$ ,  $Ga_4O_2$ ,  $In_4O_2$ , and  $Te_4O_2$  are semiconductors with band gaps ranging from 1.49 to 4.26 eV, which can be comparable to the values of other predicted semiconducting 2D metal oxides (in the range of 1.22–6.48 eV) in our previous work [8]. Especially,  $Al_4O_2$ ,  $Ga_4O_2$ , and  $In_4O_2$  possess direct band gaps, desired by optical devices. Remarkably, our cluster-assembled  $B_4O_2$  monolayer possesses a wide band gap of about 4.26 eV, rather than the metallic nature for the previously proposed  $B_2O$  monolayer and bulk systems [54–56]. From analysis of the LDOS of  $B_4O_2$ , the bottom conduction band stems mainly from the  $2p$  orbitals of B atoms and partially from the  $2p$  orbitals of O atoms, whereas the  $2p$  orbitals of O and B atoms together contribute to the top valence band. Furthermore, the substantial overlap of LDOS near the Fermi level implies strong hybridization between the orbitals of B and O atoms, i.e., stable B–O bonding. Such wide-gap semiconductors are potentially useful for electronic and optoelectronic devices to operate at much higher voltages, frequencies, and temperatures than the conventional semiconductor materials, such as silicon and gallium arsenide [67–70].

Based on the band structures, the carrier effective masses were calculated for the semiconducting 2D assemblies, summarized in Table I. The effective masses are in the range of 0.26–6.36  $m_0$  for holes, and 0.24–5.33  $m_0$  for electrons, respectively. The lower limit of the effective mass (0.24  $m_0$ ) indicates that the carriers in some of these 2D sheets are rather mobile. Additionally, there are large differences between hole and electron effective masses, which can be utilized to separate electrons and holes in electronics. Furthermore, these assembled monolayers present good optical absorption behavior. The optical absorption coefficients are obtained by computing the complex dielectric functions based on the HSE06 functional as depicted in Fig. 5(d). The semiconducting  $M_4O_2$  monolayers exhibit strong optical absorption in the visible and ultraviolet regimes with the absorption coefficient up to  $10^5 \text{ cm}^{-1}$ . Moreover, the band-edge positions of these assembled 2D semiconductors can straddle the water oxidation and reduction redox potentials (Fig. S10 of the Supplemental Material) [42]. Therefore,  $B_4O_2$ ,  $Al_4O_2$ ,  $Ga_4O_2$ ,  $In_4O_2$ , and  $Te_4O_2$  monolayers have a wide range of applications from electronics, optoelectronics, and optics to photocatalysis of water splitting.

#### IV. CONCLUSION

To summarize, we proposed a simple strategy for assembling stable 2D materials using tetrahedral clusters linked by O atoms, based on the criteria of close shells of molecular and atomic orbitals for the cluster and O atom, respectively, as well as proper electron transfer between them. Following this assembling rule, the tetrahedral clusters of group-III A (B, Al, Ga, and In), group-VIB (Cr and Mo), and group-VIA (Te) elements were selected to assemble oxide monolayers in the form of  $M_4O_2$ . For all these 2D structures, the  $M_4$  unit carries either 8 or 20 magic numbers of valence electrons after donating four electrons to the neighboring O atoms, thereby satisfying the superatomic orbital configurations by considering  $T_d$  symmetry within the shell model. These cluster-assembled monolayers are dynamically stable and robust at room

temperature. The assembled  $B_4O_2$  and  $Te_4O_2$  monolayers are demonstrated as their ground-state structures, suggesting the feasibility for experimental synthesis of these 2D materials. In addition, their physical properties are suitable for many device applications: wide band gaps ranging from 1.49 to 4.26 eV, small carrier effective masses as low as  $0.24 m_0$  and strong optical absorbance in the ultraviolet-visible regime. These theoretical results open unprecedented opportunities for the discovery of new materials and exploiting atomic clusters for assembling devices with advanced functionalities.

## ACKNOWLEDGMENTS

This work was supported by the National Natural Science Foundation of China (Grants No. 12004065, No. 91961204, and No. 11974068), the Liaoning Provincial Natural Science Foundation of China (Grant No. 2019JH3/30100002), XingLiaoYingCai Project of Liaoning Province, China (Grant No. XLYC1905014). We acknowledge the computer resources provided by the Supercomputing Center of Dalian University of Technology and Shanghai Supercomputer Center.

- [1] J. Zhao, H. Liu, Z. Yu, R. Quhe, S. Zhou, Y. Wang, C. C. Liu, H. Zhong, N. Han, and J. Lu, Rise of silicene: A competitive 2D material, *Prog. Mater. Sci.* **83**, 24 (2016).
- [2] Y. Guo, S. Zhou, and J. Zhao, Two-dimensional intrinsic ferromagnets with high Curie temperatures: Synthesis, physical properties and device applications, *J. Mater. Chem. C* **9**, 6103 (2021).
- [3] X. Liu and M. C. Hersam, 2D materials for quantum information science, *Nat. Rev. Mater.* **4**, 669 (2019).
- [4] D. Zhou, H. Li, N. Si, H. Li, H. Fuchs, and T. Niu, Epitaxial growth of maingroup mono-elemental 2D materials, *Adv. Funct. Mater.* **31**, 2006997 (2021).
- [5] N. R. Glavin, R. Rao, V. Varshney, E. Bianco, A. Apte, A. Roy, E. Ringe, and P. M. Ajayan, Emerging applications of elemental 2D materials, *Adv. Mater.* **32**, 1904302 (2020).
- [6] S. Yu, X. Wu, Y. Wang, X. Guo, and L. Tong, 2D materials for optical modulation: Challenges and opportunities, *Adv. Mater.* **29**, 1606128 (2017).
- [7] M. Gibertini, M. Koperski, A. F. Morpurgo, and K. S. Novoselov, Magnetic 2D materials and heterostructures, *Nat. Nanotechnol.* **14**, 408 (2019).
- [8] Y. Guo, L. Ma, K. Mao, M. Ju, Y. Bai, J. Zhao, and X. C. Zeng, Eighteen functional monolayer metal oxides: Wide bandgap semiconductors with superior oxidation resistance and ultrahigh carrier mobility, *Nanoscale Horiz.* **4**, 592 (2019).
- [9] Y. Guo, Q. Wu, Y. Li, N. Lu, K. Mao, Y. Bai, J. Zhao, J. Wang, and X. C. Zeng, Copper(i) sulfide: A two-dimensional semiconductor with superior oxidation resistance and high carrier mobility, *Nanoscale Horiz.* **4**, 223 (2019).
- [10] K. S. Burch, D. Mandrus, and J.-G. Park, Magnetism in two-dimensional van der Waals materials, *Nature (London)* **563**, 47 (2018).
- [11] W. Liu, J. Hu, S. Zhang, M. Deng, C.-G. Han, and Y. Liu, New trends, strategies, and opportunities in thermoelectric materials: A perspective, *Mater. Today Phys.* **1**, 50 (2017).
- [12] A. Zunger, Inverse design in search of materials with target functionalities, *Nat. Rev. Chem.* **2**, 0121 (2018).
- [13] J. Zhao, Q. Du, S. Zhou, and V. Kumar, Endohedrally doped cage clusters, *Chem. Rev.* **120**, 9021 (2020).
- [14] S. A. Claridge, A. W. Castleman Jr, S. N. Khanna, C. B. Murray, A. Sen, and P. S. Weiss, Cluster-assembled materials, *ACS Nano* **3**, 244 (2009).
- [15] M. Qian, A. C. Reber, A. Ugrinov, N. K. Chaki, S. Mandal, H. M. Saavedra, S. N. Khanna, A. Sen, and P. S. Weiss, Cluster-assembled materials: Toward nanomaterials with precise control over properties, *ACS Nano* **4**, 235 (2010).
- [16] S. Mandal, A. C. Reber, M. Qian, R. Liu, H. M. Saavedra, S. Sen, P. S. Weiss, S. N. Khanna, and A. Sen, Synthesis, structure and band gap energy of covalently linked cluster-assembled materials, *Dalton Trans.* **41**, 12365 (2012).
- [17] S. D. Korlann, A. E. Riley, B. S. Mun, and S. H. Tolbert, Chemical tuning of the electronic properties of nanostructured semiconductor films formed through surfactant templating of zinc cluster, *J. Phys. Chem. C* **113**, 7697 (2009).
- [18] H. Xu, Y. Hou, and H. Zhang, CdTe magic-sized clusters and the use as building blocks for assembling two-dimensional nanoplatelets, *J. Nanopart. Res.* **19**, 189 (2017).
- [19] X. Zhong, K. Lee, B. Choi, D. Meggiolaro, F. Liu, C. Nuckolls, A. Pasupathy, F. De Angelis, P. Batail, and X. Roy, Superatomic two-dimensional semiconductor, *Nano Lett.* **18**, 1483 (2018).
- [20] E. J. Telford, J. C. Russell, J. R. Swann, B. Fowler, X. Wang, K. Lee, A. Zangiabadi, K. Watanabe, T. Taniguchi, and C. Nuckolls, Doping-induced superconductivity in the van der Waals superatomic crystal  $Re_6Se_8Cl$ , *Nano Lett.* **20**, 1718 (2020).
- [21] B. Choi, K. Lee, A. Voevodin, J. Wang, M. L. Steigerwald, P. Batail, X. Zhu, and X. Roy, Two-dimensional hierarchical semiconductor with addressable surfaces, *J. Am. Chem. Soc.* **140**, 9369 (2018).
- [22] J. Y. Wang, R. W. Huang, Z. Wei, X. Dong, and S. Q. Zang, Linker flexibility-dependent cluster transformations and cluster-controlled luminescence in isostructural silver cluster-assembled materials (SCAMs), *Chem. European J.* **25**, 3376 (2019).
- [23] K. Lee, B. Choi, I. J. L. Plante, M. V. Paley, X. Zhong, A. C. Crowther, J. S. Owen, X. Zhu, and X. Roy, Two-dimensional fullerene assembly from an exfoliated van der Waals template, *Angew. Chem., Int. Ed.* **130**, 6233 (2018).
- [24] X. Roy, C.-H. Lee, A. C. Crowther, C. L. Schenck, T. Besara, R. A. Lalancette, T. Siegrist, P. W. Stephens, L. E. Brus, and P. Kim, Nanoscale atoms in solid-state chemistry, *Science* **341**, 157 (2013).
- [25] Q. Du, Z. Wang, S. Zhou, J. Zhao, and V. Kumar, Searching for cluster Lego blocks for three-dimensional and two-dimensional assemblies, *Phys. Rev. Mater.* **5**, 066001 (2021).
- [26] T. Tsukamoto, N. Haruta, T. Kambe, A. Kuzume, and K. Yamamoto, Periodicity of molecular clusters based on symmetry-adapted orbital model, *Nat. Commun.* **10**, 3727 (2019).
- [27] R. O. Jones and D. Hohl, Structure of phosphorus clusters using simulated annealing— $P_2$  to  $P_8$ , *J. Chem. Phys.* **92**, 6710 (1990).

- [28] A. Rodin, A. Carvalho, and A. C. Neto, Strain-Induced Gap Modification in Black Phosphorus, *Phys. Rev. Lett.* **112**, 176801 (2014).
- [29] W. Kohn and L. J. Sham, Self-consistent equations including exchange and correlation effects, *Phys. Rev.* **140**, A1133 (1965).
- [30] G. Kresse and J. Furthmüller, Efficient iterative schemes for ab initio total-energy calculations using a plane-wave basis set, *Phys. Rev. B* **54**, 11169 (1996).
- [31] P. E. Blöchl, Projector augmented-wave method, *Phys. Rev. B* **50**, 17953 (1994).
- [32] G. Kresse and D. Joubert, From ultrasoft pseudopotentials to the projector augmented-wave method, *Phys. Rev. B* **59**, 1758 (1999).
- [33] J. P. Perdew, K. Burke, and M. Ernzerhof, Generalized Gradient Approximation Made Simple, *Phys. Rev. Lett.* **77**, 3865 (1996).
- [34] J. Heyd, G. E. Scuseria, and M. Ernzerhof, Hybrid functionals based on a screened Coulomb potential, *J. Chem. Phys.* **118**, 8207 (2003).
- [35] S. Baroni, S. de Gironcoli, A. Dal Corso, and P. Giannozzi, Phonons and related crystal properties from density-functional perturbation theory, *Rev. Mod. Phys.* **73**, 515 (2001).
- [36] R. Krishnan, J. S. Binkley, R. Seeger, and J. A. Pople, Self-consistent molecular orbital methods. XX. A basis set for correlated wave functions, *J. Chem. Phys.* **72**, 650 (1980).
- [37] M. Dolg, U. Wedig, H. Stoll, and H. Preuss, Energy-adjusted abinitio pseudopotentials for the first row transition elements, *J. Chem. Phys.* **86**, 866 (1987).
- [38] M. J. Frisch, G. W. Trucks, H. B. Schlegel, G. E. Scuseria, M. A. Robb, J. R. Cheeseman, G. Scalmani, V. Barone, G. A. Petersson, and H. Nakatsuji, *Gaussian, 16 version* (Gaussian Inc., Wallingford, CT, 2016).
- [39] Y. Wang, M. Miao, J. Lv, L. Zhu, K. Yin, H. Liu, and Y. Ma, An effective structure prediction method for layered materials based on 2D particle swarm optimization algorithm, *J. Chem. Phys.* **137**, 224108 (2012).
- [40] Y. Wang, J. Lv, L. Zhu, and Y. Ma, Crystal structure prediction via particle-swarm optimization, *Phys. Rev. B* **82**, 094116 (2010).
- [41] M. Brack, The physics of simple metal clusters: Self-consistent jellium model and semiclassical approaches, *Rev. Mod. Phys.* **65**, 677 (1993).
- [42] See Supplemental Material at <http://link.aps.org/supplemental/10.1103/PhysRevResearch.3.043231> for the stability of  $\text{Ti}_4\text{O}_2$  and  $\text{W}_4\text{O}_2$  monolayers, several  $\text{M}_2\text{O}$  monolayers without tetrahedral clusters, previously proposed  $\text{B}_2\text{O}$  systems, AIMD snapshots of assemblies of tetrahedral cluster taken at the end of the simulation, geometric structures of selected  $\text{B}_4\text{O}_2$  and  $\text{Te}_4\text{O}_2$ , and phonon dispersions, ELF, electronic structures and band edges of assembled monolayers.
- [43] D. Schattschneider, The plane symmetry groups: Their recognition and notation, *Am. Math. Monthly* **85**, 439 (1978).
- [44] F. A. Cotton and D. G. Nocera, The whole story of the two-electron bond, with the  $\delta$  bond as a paradigm, *Accounts Chem. Res.* **33**, 483 (2000).
- [45] X. Huang, H. J. Zhai, B. Kiran, and L. S. Wang, Observation of d-orbital aromaticity, *Angew. Chem., Int. Ed.* **117**, 7417 (2005).
- [46] H.-J. Zhai, W.-J. Chen, X. Huang, and L.-S. Wang, On the electronic structure and conflicting d-orbital aromaticity in the  $\text{Re}_3\text{O}_3^-$  cluster, *RSC Adv.* **2**, 2707 (2012).
- [47] F. L. Hirshfeld, Bonded-atom fragments for describing molecular charge densities, *Theor. Chim. Acta* **44**, 129 (1977).
- [48] N. C. Bacalis, A. Metropoulos, and A. Gross, Theoretical study of the  $\text{O}_2$  interaction with a tetrahedral  $\text{Al}_4$  cluster, *J. Phys. Chem. A* **114**, 11746 (2010).
- [49] M. A. Shestopalov, A. Y. Ledneva, S. Cordier, O. Hernandez, M. Potel, T. Roisnel, N. G. Naumov, and C. Perrin, Tetrahedral  $\text{Mo}_4$  clusters as building blocks for the design of clathrate-related giant frameworks, *Angew. Chem., Int. Ed.* **123**, 7438 (2011).
- [50] O. López-Estrada, S. López-Olay, A. Aburto, and E. Orgaz, Unexpected high spin polarization in  $\text{Cr}_4$  cluster, *J. Phys. Chem. C* **120**, 23892 (2016).
- [51] H. Reis and M. G. Papadopoulos, Nonlinear optical properties of the rhombic  $\text{B}_4$ -cluster, *J. Comput. Chem.* **20**, 679 (1999).
- [52] U. Meier, S. Peyerimhoff, and F. Grein, ab initio MRD-CI study of neutral and charged  $\text{Ga}_2$ ,  $\text{Ga}_3$  and  $\text{Ga}_4$  clusters and comparison with corresponding boron and aluminum clusters, *Z. Phys. D: At., Mol. Clusters* **17**, 209 (1990).
- [53] L. Tan, L. Huang, C. He, J. C. Mauro, M. Peng, X.-B. Yang, and Y. Yue, Tailoring cluster configurations enables tunable broadband luminescence in glass, *Chem. Mater.* **32**, 8653 (2020).
- [54] C. Zhong, W. Wu, J. He, G. Ding, Y. Liu, D. Li, S. A. Yang, and G. Zhang, Two-dimensional honeycomb borophene oxide: Strong anisotropy and nodal loop transformation, *Nanoscale* **11**, 2468 (2019).
- [55] X. Zhao, X. Yang, D. Singh, P. K. Panda, W. Luo, Y. Li, and R. Ahuja, Strain-engineered metal-free h- $\text{B}_2\text{O}$  monolayer as a mechanocatalyst for photocatalysis and improved hydrogen evolution reaction, *J. Phys. Chem. C* **124**, 7884 (2020).
- [56] K. Persson, Materials data on  $\text{B}_2\text{O}$  (SG:164) by Materials Project (2016), doi: [10.17188/1277769](https://doi.org/10.17188/1277769).
- [57] G. Kresse and J. Hafner, *Ab initio* molecular dynamics for liquid metals, *Phys. Rev. B* **47**, 558(R) (1993).
- [58] K. E. Schriver, J. L. Persson, E. C. Honea, and R. Whetten, Electronic Shell Structure of Group-III A Metal Atomic Clusters, *Phys. Rev. Lett.* **64**, 2539 (1990).
- [59] W. A. Heer, The physics of simple metal clusters: Experimental aspects and simple models, *Rev. Mod. Phys.* **65**, 611 (1993).
- [60] Q. Sun, Q. Wang, J. Yu, V. Kumar, and Y. Kawazoe, Real-space representation of electron localization and shell structure in jelliumlike clusters, *Phys. Rev. B* **63**, 193408 (2001).
- [61] P. Jena and Q. Sun, Super atomic clusters: Design rules and potential for building blocks of materials, *Chem. Rev.* **118**, 5755 (2018).
- [62] S. G. Frauendorf and C. Guet, Atomic clusters as a branch of nuclear physics, *Annu. Rev. Nucl. Part. Sci.* **51**, 219 (2001).
- [63] Y. Jia and Z. Luo, Thirteen-atom metal clusters for genetic materials, *Coord. Chem. Rev.* **400**, 213053 (2019).
- [64] Z. Luo, G. U. Gamboa, J. C. Smith, A. C. Reber, J. U. Reveles, S. N. Khanna, and A. W. Castleman, Spin accommodation and reactivity of silver clusters with oxygen: The enhanced stability of  $\text{Ag}_{13}^-$ , *J. Am. Chem. Soc.* **134**, 18973 (2012).
- [65] Z. Luo and A. W. Castleman, Special and General Superatoms, *Acc. Chem. Res.* **47**, 2931 (2014).
- [66] A. C. Reber and S. N. Khanna, Superatoms: Electronic and geometric effects on reactivity, *Acc. Chem. Res.* **50**, 255 (2017).

- [67] T. P. Chow and R. Tyagi, Wide bandgap compound semiconductors for superior high-voltage unipolar power devices, *IEEE Trans. Electron Devices* **41**, 1481 (1994).
- [68] P. G. Neudeck, R. S. Okojie, and C. Liang-Yu, High-temperature electronics - a role for wide bandgap semiconductors?, *Proc. IEEE* **90**, 1065 (2002).
- [69] J. L. Hudgins, G. S. Simin, E. Santi, and M. A. Khan, An assessment of wide bandgap semiconductors for power devices, *IEEE Trans. Power Electron.* **18**, 907 (2003).
- [70] E. Monroy, F. Omnès, and F. Calle, Wide-bandgap semiconductor ultraviolet photodetectors, *Semicond. Sci. Technol.* **18**, R33 (2003).